Contact modelling using Trefftz and interface finite elements

Ke Y. Wang, Manicka Dhanasekar*, Jian J. Han

Centre for Railway Engineering
Central Queensland University, QLD 4702, Australia
e-mail: m.dhanasekar@cqu.edu.au

Qing H. Qin

Department of Engineering
Australian National University, ACT0200, Australia
e-mail: qinghua.qin@anu.edu.au

Yi L. Kang

Department of Mechanics
Tianjin University, 300072, PR China.

Abstract

Modelling of elastic contact problems is addressed with the aid of Hybrid-Trefftz (HT) and interface finite elements based on a simple interfacial constitutive relation. This paper presents the formulation of a four-noded HT finite element for discretizing the contacting bodies and a four-noded interface element that could be embedded in the prospective contact zone for simulating the interaction behaviour. Due to the superior performance, the Simpson-type Newton-Cotes integration scheme is utilized to compute interface element formulation numerically. In order to evaluate the applicability of the present approach two benchmark examples are investigated in detail. Comparisons have been made between the results by the present approach and analytical as well as traditional FE solutions using ABAQUS software.

1 Introduction

Contact problems have attracted much attention due to their inherent complexity and frequent occurrence in engineering practice. A variety of numerical approaches for calculating contact zones, and dividing them into stick and slip subzones, as well as determining the contact stresses, are available in the literature. Amongst these approaches the interface element (IE) methodology, due to its ease of numerical implementation, has been investigated by many researchers. Goodman et al [1] presented the pioneering work on such an element for evaluating the behaviour of jointed rock mass. However, the kinematic inconsistency associated with this element usually has resulted in spurious oscillations of tangential traction. To circumvent this difficulty, the Newton-Cotes integration scheme was used by several authors instead of the widely adopted Gaussian quadrature [2,4,5]. Day and Potts [2] argued that the reduced Gauss integration used by Gens et al [3] could not avoid the instability of the traction profile. Lei [4] illustrated the performance of Newton-Cotes integration scheme through two examples of a smooth footing on elastic sub-soil and a pull-out problem. Schellekens and De Borst [5] specially discussed this integration scheme and provided an explanation for some numerical results. They pointed out that, for either linear or quadratic interface elements, the aforementioned instabilities can not be recovered in the case of high gradient tractions. Therefore, other types [6,7] of interface element were subsequently proposed in the literature. Herrmann [6] assumed each pair of matching nodes has been linked through fictitious springs - one normal and the other tangential to the interface. Although such treatment overcomes the disadvantage occurring in Goodman-type element, the uncoupling between links does not accord totally with the practice and often leads to unreliable normal response. In the light of this, Kaliakin and Li [7] have developed an improved type of element which possesses the normal response

characteristics of the Goodman element, and eliminates the kinematic deficiencies by employing tangential response similar to the Herrmann element [6].

As a promising technique for the numerical solution of a variety of problems encountered in engineering, HT FE approach assimilates the merits of the conventional FE and boundary element (BE) methods and, moreover, discards some of their drawbacks [8]: Firstly, the element formulation calls for integration along the element boundaries only, and secondly, some problems with singular or local effects can be treated easily if exact local solution functions are available. A general purpose HT FE formulation was first developed by Jirousek and Leon [9] who studied the effect of mesh distortion on thin plate elements. Since then, the HT element concept has become increasingly popular, attracting a growing number of researchers into this field [8]. So far, HT elements have been successfully applied to numerous problems such as elasticity [10,11], elastoplasticity [12,13], plates [14,15], transient heat conduction analysis [16] and piezoelectric materials [17,18]. According to authors' knowledge, there are only a few papers [19,20] reporting application of HT FE technique to contact problems in the literature. Hochard [19] dealt with frictionless contact between an elastic domain and a rigid support by transforming the equations of contact to a problem of minimization under linear constraints. Recently, Wang et al [20] developed a HT FE interface model for contact problems with the aid of direct constraint approach.

The purpose of this paper is to develop a HT FE model and apply it to elastic contact problems with the help of Kaliakin-Li (KL) interface elements [7]. In the model, a 4-node HT element has been formulated and applied for discretizing both contacting bodies; 4-node KL elements have been embedded for simulating the potential contact zone. To assess the reliability of the KL elements for predicting the contact behaviour, an interfacial constitutive relation, namely penalized normal contact and tangential friction law, has been adopted. In addition, the Simpson-type Newton-Cotes integration scheme [21] is recommended to evaluate the formulation of the KL element in this analysis. The HT FE-interface model presented in this paper has been implemented into a commercial FE package, ABAQUS, via user element subroutine (UEL). Two benchmark examples have been presented to illustrate the applicability of the overall model to contact problems. Good agreements have been achieved between the results from the present approach and analytical as well as the conventional FE solutions obtained from ABAQUS software.

2 Hybrid Trefftz and interface element model

2.1 HT element formulation

Fig.1 shows two linear elastic bodies Ω^A and Ω^B in closer contact. The boundary Γ^α of each body Ω^α $(\alpha = A, B)$ consists of three disjointed portions Γ_u^α, Γ_t^α and Γ_c^α. Γ_u^α and Γ_t^α are respectively

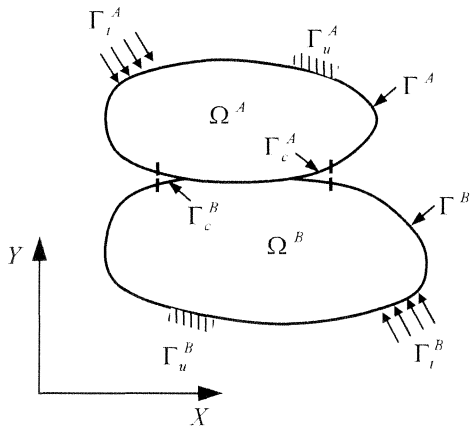

Fig. 1 Graphic representation of contact problem

prescribed displacement and traction boundaries, Γ_c^{α} represents the prospective contact surface of each body which should be assumed large enough to contain the actual contact surface after deformation. The basic equations of HT FE model in the global Cartesian coordinates $X_i (i = 1, 2)$ are summarized as follows:

$$\sigma_{ij,j} + \bar{b}_i = 0 \qquad \text{in } \Omega^A \cup \Omega^B \tag{1a}$$

$$\left.\begin{aligned} \sigma_{ij} &= D_{ijkl}\varepsilon_{kl} \\ \varepsilon_{ij} &= C_{ijkl}\sigma_{kl} \\ \varepsilon_{ij} &= \tfrac{1}{2}\left(u_{i,j} + u_{j,i}\right) \end{aligned}\right\} \quad \text{in } \Omega^A \cup \Omega^B \tag{1b}$$

$$u_i = \bar{u}_i \qquad \text{on } \Gamma_u^A \cup \Gamma_u^B \tag{1c}$$

$$t_i = \sigma_{ij} n_j = \bar{t}_i \qquad \text{on } \Gamma_t^A \cup \Gamma_t^B \tag{1d}$$

$$u_{ia} = u_{ib} \qquad \text{on } \Gamma_a \cap \Gamma_b \tag{1e}$$

$$t_{ia} + t_{ib} = 0 \qquad \text{on } \Gamma_a \cap \Gamma_b \tag{1f}$$

Eqs.(1a-d) are the fundamental relations of conventional FEM, while Eqs.(1e,1f) are additional inter-element continuity requirements for HT FEM. Where σ_{ij} and ε_{ij} are respectively the stress and strain tensors, D_{ijkl} and C_{ijkl} the stiffness and compliance coefficient tensors, u_i, t_i and b_i denote respectively displacements, tractions and body forces and overhead bar stands for prescribed value, n_j stand for direction cosines of the outward normal at a given point on the boundary, subscripts "a" and "b" represent any two adjacent elements.

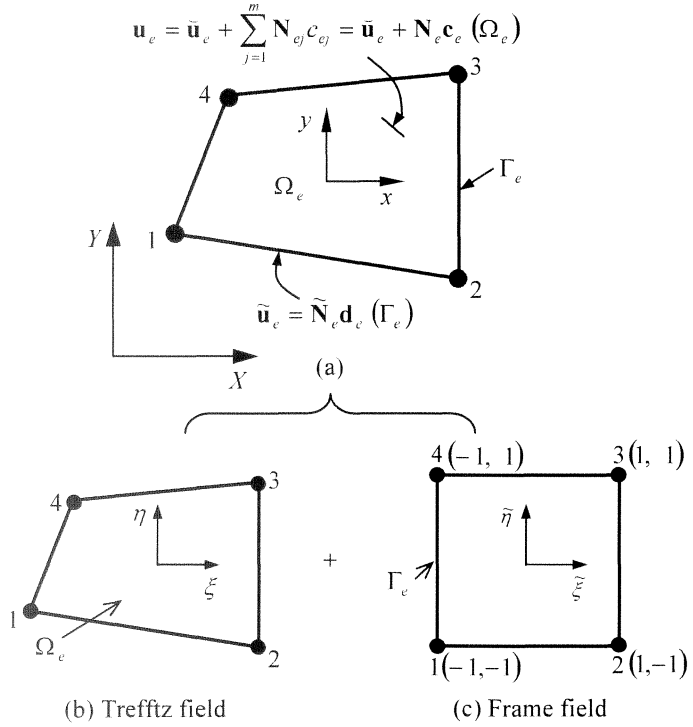

Fig. 2 Four-noded HT element

To establish the formulation for a particular HT element 'e', two groups of distinct displacement fields [11] (see Fig.2):

(i) a nonconforming intra-element displacement field (Trefftz field)

$$\mathbf{u}_e = \breve{\mathbf{u}}_e + \sum_{j=1}^{m} \mathbf{N}_{ej} c_{ej} = \breve{\mathbf{u}}_e + \mathbf{N}_e \mathbf{c}_e \quad \text{in } \Omega_e \tag{2a}$$

(ii) an exactly and minimally conforming auxiliary frame field

$$\widetilde{\mathbf{u}}_e = \widetilde{\mathbf{N}}_e \mathbf{d}_e \quad \text{on } \Gamma_e \tag{2b}$$

are assumed on the basis of the Trefftz method. Where $\breve{\mathbf{u}}_e$ and $\mathbf{N}_e$ are, respectively, the particular and homogeneous solutions (so-called Trefftz functions) to Eq.(1a), $\mathbf{c}_e$ is a vector of unknown parameters, m is the number of Trefftz solutions, $\widetilde{\mathbf{N}}_e$ are the shape functions (frame functions) defined in the customary way, the tilde appearing in Eq.(2b) indicates that the frame field is defined on the element boundary only.

A complete system of Trefftz functions $\mathbf{N}_e$ may be generated with the aid of Muskhelish's of complex variable formulation. The results presented in [11] are listed in Appendix A. It is important to determine the optimal value of m with respect to accuracy and computational effort in HT FE analysis. Wang et al [20] stated that the choice of m =9 can produce robust 4-node plane HT element so that

$$\mathbf{N}_e = \mathbf{N}_e(x, y) = \frac{1}{2G}\begin{bmatrix} (\kappa-1)x & y & -x & -2\kappa xy & (\kappa-2)x^2 - (\kappa+2)y^2 \\ (\kappa-1)y & x & y & (\kappa+2)x^2 - (\kappa-2)y^2 & 2\kappa xy \end{bmatrix}$$

$$\begin{bmatrix} 2xy & y^2 - x^2 & (3-3\kappa)x^2 y + (\kappa+3)y^3 & (\kappa-3)x^3 - (3\kappa+3)xy^2 \\ x^2 - y^2 & 2xy & (\kappa+3)x^3 - (3\kappa-3)xy^2 & (3\kappa+3)x^2 y - (\kappa-3)y^3 \end{bmatrix} \tag{3}$$

where $G = E/(2+2\nu)$, $\kappa = 3-4\nu$ for plane stress whereas $\kappa = (3-7\nu)/(1-\nu)$ for plane strain, E and ν are respectively Young's modulus and Poisson's ratio and (x, y) is the local Cartesian coordinate system which originates at the element centroid:

$$\begin{cases} x = X - X_o = X - \dfrac{1}{4}\displaystyle\sum_{i=1}^{4} X_i \\ y = Y - Y_o = Y - \dfrac{1}{4}\displaystyle\sum_{i=1}^{4} Y_i \end{cases} \tag{4}$$

where X_o, Y_o and X_i, Y_i are, respectively, the global Cartesian coordinates of centroid and nodes of the element. In HT FE implementation, additionally, a so-called Trefftz dimensionless coordinate system (ξ, η):

$$\xi = \frac{x}{l_e}, \eta = \frac{y}{l_e} \tag{5}$$

together with

$$l_e = \frac{1}{4}\sum_{i=1}^{4} \sqrt{x_i^2 + y_i^2} \tag{6}$$

has to be used to ensure a good numerical conditioning of the element flexibility matrix $\mathbf{H}_e$ defined below. Where l_e denotes the average distance between the element nodes and its centroid (termed element characteristic length). In practice, replacing x and y in Eq.(3) by ξ and η and extracting l_e produces

$$\mathbf{N}_e = \mathbf{N}_e(x, y) = \mathbf{N}_e(\xi, \eta)\mathbf{L}_e(l_e) \tag{7}$$

where $\mathbf{L}_e(l_e)$ is a diagonal matrix with respect to the element characteristic length; for $m = 9$, $\mathbf{L}_e(l_e) = \mathrm{diag}(l_e \quad l_e \quad l_e \quad l_e^2 \quad l_e^2 \quad l_e^2 \quad l_e^2 \quad l_e^3 \quad l_e^3)$.

According to the concept of isoparametric element, $\widetilde{\mathbf{N}}_e$ is given as

$$\widetilde{\mathbf{N}}_e = \begin{bmatrix} \widetilde{N}_1 & 0 & \widetilde{N}_2 & 0 & \widetilde{N}_3 & 0 & \widetilde{N}_4 & 0 \\ 0 & \widetilde{N}_1 & 0 & \widetilde{N}_2 & 0 & \widetilde{N}_3 & 0 & \widetilde{N}_4 \end{bmatrix} \tag{8}$$

for 4-node HT element. Here $\widetilde{N}_i(\widetilde{\xi}, \widetilde{\eta}) = \frac{1}{4}(1 + \widetilde{\xi}\widetilde{\xi}_i)(1 + \widetilde{\eta}\widetilde{\eta}_i)$ $(i = 1,2,3,4)$, $(\widetilde{\xi}, \widetilde{\eta})$ stands for isoparametric coordinate system for the frame. Alternative form of $\widetilde{\mathbf{N}}_e$ which is equivalent to Eq.(8) is used by Qin [8].

For numerical computations, it is convenient to rewrite $\widetilde{\mathbf{N}}_e(\widetilde{\xi}, \widetilde{\eta})$ in terms of ξ and η by a simple relation [22]

$$\begin{Bmatrix} \widetilde{\xi} \\ \widetilde{\eta} \end{Bmatrix} \Rightarrow \begin{Bmatrix} X = \sum_{i=1}^{4} \widetilde{N}_i(\widetilde{\xi}, \widetilde{\eta}) X_i \\ Y = \sum_{i=1}^{4} \widetilde{N}_i(\widetilde{\xi}, \widetilde{\eta}) Y_i \end{Bmatrix} \Rightarrow \begin{Bmatrix} \xi = \dfrac{x}{l_e} = \dfrac{X - X_o}{l_e} \\ \eta = \dfrac{y}{l_e} = \dfrac{Y - Y_o}{l_e} \end{Bmatrix} \tag{9}$$

and thus

$$\widetilde{\mathbf{N}}_e = \widetilde{\mathbf{N}}_e(\widetilde{\xi}, \widetilde{\eta}) = \widetilde{\mathbf{N}}_e(x, y) = \widetilde{\mathbf{N}}_e(\xi, \eta) \tag{10}$$

The corresponding traction field $\mathbf{t}_e$ can be derived from Eqs.(1b,d) and (2a) such that

$$\mathbf{t}_e = \bar{\mathbf{t}}_e + \sum_{j=1}^{m} \mathbf{Q}_{ej} c_j = \bar{\mathbf{t}}_e + \mathbf{Q}_e \mathbf{c}_e \tag{11}$$

where $\mathbf{Q}_e = \mathbf{ADLN}_e$, in which $\mathbf{A}$, $\mathbf{D}$ and $\mathbf{L}$ are transformation, constitutive and differential operator matrices respectively [8].

According to the modified variational principles presented by Qin [23]

$$\Pi_m = \sum_e \Pi_{me} = \sum_e \left[\Pi_e - \int_{\Gamma_{eu}} (t_i - \bar{t}_i)\widetilde{u}_i \, \mathrm{d}\Gamma - \int_{\Gamma_{el}} t_i \widetilde{u}_i \, \mathrm{d}\Gamma \right] \tag{12a}$$

$$\Psi_m = \sum_e \Psi_{me} = \sum_e \left[\Psi_e - \int_{\Gamma_{et}} (u_i - \bar{u}_i)\widetilde{t}_i \, \mathrm{d}\Gamma - \int_{\Gamma_{el}} t_i \widetilde{u}_i \, \mathrm{d}\Gamma \right] \tag{12b}$$

where Π_e and Ψ_e are, respectively, the minimum potential and complementary functionals, $\Gamma_e = \Gamma_{eu} \cup \Gamma_{et} \cup \Gamma_{el}$, while $\Gamma_{eu} = \Gamma_u \cap \Gamma_e$, $\Gamma_{et} = \Gamma_t \cap \Gamma_e$, and Γ_{el} is the inter-element boundary of element 'e'.

Taking the vanishing variation of (12a) or (12b) we can readily obtain the customary force-displacement relationship, i.e. the element stiffness equation as

$$\mathbf{K}_e \mathbf{d}_e = \mathbf{P}_e \tag{13}$$

where

$$\mathbf{K}_e = \mathbf{G}_e^T \mathbf{H}_e^{-1} \mathbf{G}_e \tag{14a}$$

$$\mathbf{P}_e = \mathbf{G}_e^T \mathbf{H}_e^{-1} \mathbf{h}_e + \mathbf{g}_e \tag{14b}$$

The derivation of the element stiffness equation from (12a) and the expressions for auxiliary matrices $\mathbf{H}_e$, $\mathbf{G}_e$, $\mathbf{h}_e$ and $\mathbf{g}_e$ are addressed in Appendix B.

By using Eqs.(7) and (10) and making some manipulation, we obtain the following expressions of $\mathbf{K}_e$ and $\mathbf{P}_e$:

$$\mathbf{K}_e = \mathbf{K}_e(x, y) = \mathbf{K}_e(\xi, \eta) \tag{15a}$$

$$\mathbf{P}_e = \mathbf{P}_e(x, y) = \mathbf{P}_e(\xi, \eta) \tag{15b}$$

It is obviously noted that $\mathbf{K}_e$ and $\mathbf{P}_e$ remain truly unchanged in their magnitude from the local Cartesian coordinate system to the Trefftz dimensionless one. Therefore, we can use the right hand side of Eqs.(15a,b) to evaluate the HT element stiffness equation directly.

2.2 KL interface element formulation

For completeness, an improved interface element proposed by Kalakin and Li [7] is briefly reviewed. A representative 4-node KL interface element is depicted in Fig.3. Such element possesses zero thickness before deformation.

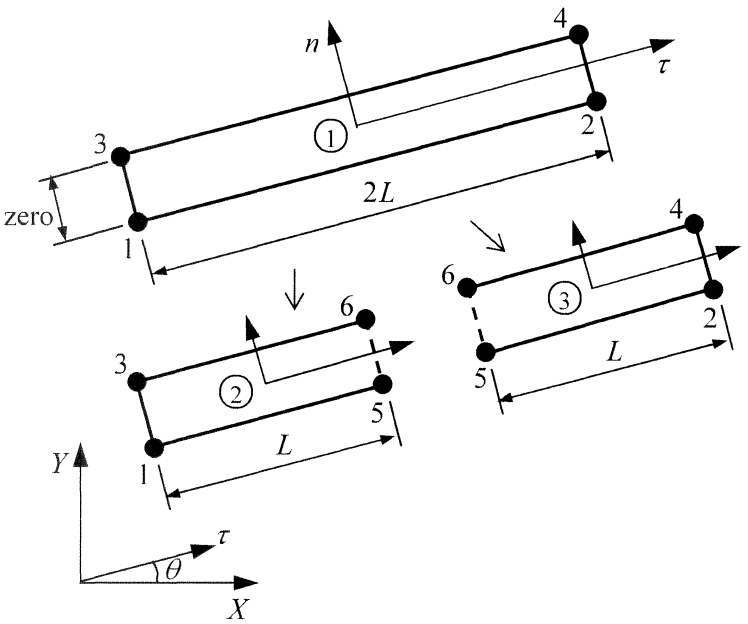

Fig. 3 Four-noded KL interface element

In order to derive the element formulation KL element 1-2-3-4 (denoted by ①) is decomposed into two sub elements 1-5-3-6 (denoted by ②) and 5-2-6-4 (denoted by ③) in Fig.3. Adopting the idea of Goodman et al [1], the relative displacement vector, $\hat{\mathbf{w}} = (\hat{w}_\tau \quad \hat{w}_n)^T$, at any generic point of interface with respect to the local system (τ, n) may be defined as

$$\hat{\mathbf{w}} = \begin{Bmatrix} \hat{w}_\tau \\ \hat{w}_n \end{Bmatrix} = \begin{Bmatrix} u_\tau^{top} - u_\tau^{bot} \\ u_n^{top} - u_n^{bot} \end{Bmatrix} = \mathbf{\Phi}\hat{\mathbf{d}}'_e \tag{16}$$

where

$$\mathbf{\Phi} = -\mathbf{M} \vdots \mathbf{M} \quad \text{with } \mathbf{M} = \begin{bmatrix} m_1 & 0 & m_2 & 0 \\ 0 & m_2 & 0 & m_2 \end{bmatrix} \tag{17a}$$

$$\hat{\mathbf{d}}'_e = \{u_{1\tau} \quad u_{1n} \quad u_{2\tau} \quad u_{2n} \quad u_{3\tau} \quad u_{3n} \quad u_{4\tau} \quad u_{4n}\}^T \tag{17b}$$

in which $m_1 = \frac{1}{2}(1-\zeta)$, $m_2 = \frac{1}{2}(1+\zeta)$, the superscript $\wedge$ stands for variables of the interface.

Accordingly, the traction vector, $\hat{\boldsymbol{\sigma}} = \{\hat{\sigma}_\tau \quad \hat{\sigma}_n\}^T$, is readily expressed as

$$\hat{\boldsymbol{\sigma}} = \mathbf{D}\hat{\mathbf{w}} = \mathbf{D}\boldsymbol{\Phi}\hat{\mathbf{d}}'_e \tag{18}$$

where $\mathbf{D} = \mathrm{diag}(k_\tau \quad k_n)$ is the interfacial constitutive matrix, k_τ and k_n are respectively the tangential and normal penalty stiffness parameters of the interface.

By using the virtual work principle, the stiffness equation of the Goodman-type element in the local system is defined as

$${}^*\hat{\mathbf{K}}'_e\,{}^*\hat{\mathbf{d}}'_e = {}^*\hat{\mathbf{P}}'_e \tag{19}$$

together with

$${}^*\hat{\mathbf{K}}'_e = \frac{L}{2}\int_{-1}^{+1}\boldsymbol{\Phi}^T\mathbf{D}\boldsymbol{\Phi}d\zeta, \quad {}^*\hat{\mathbf{P}}'_e = \frac{L}{2}\int_{-1}^{+1}\boldsymbol{\Phi}^T\hat{\boldsymbol{\sigma}}d\zeta, \quad {}^*\hat{\mathbf{d}}'_e = \text{Eq.}(17b) \tag{20a,b}$$

It is worth noting that the integrals appearing in the above equation are performed by the Simpson-type of the Newton-Cotes integration scheme. All types of this scheme are provided in Appendix C. Next, using standard assembly procedure the stiffness equations of elements ② and ③ can be combined into a form

$${}^{**}\hat{\mathbf{K}}'_e\,{}^{**}\hat{\mathbf{d}}'_e = {}^{**}\hat{\mathbf{P}}'_e \tag{21}$$

where

$${}^{**}\hat{\mathbf{d}}'_e = \{u_{1\tau} \quad u_{1n} \quad u_{2\tau} \quad u_{2n} \quad u_{3\tau} \quad u_{3n} \quad u_{4\tau} \quad u_{4n} \quad u_{5\tau} \quad u_{5n} \quad u_{6\tau} \quad u_{6n}\}^T \tag{22}$$

Eq.(21) can also be written in terms of submatrices as

$$\begin{bmatrix}\hat{\mathbf{K}}_{rr} & \hat{\mathbf{K}}_{rc}\\ \hat{\mathbf{K}}_{cr} & \hat{\mathbf{K}}_{cc}\end{bmatrix}\begin{Bmatrix}\hat{\mathbf{d}}_r\\ \hat{\mathbf{d}}_c\end{Bmatrix} = \begin{Bmatrix}\hat{\mathbf{P}}_r\\ \hat{\mathbf{P}}_c\end{Bmatrix} \tag{23}$$

where subscript c stands for variables associated with nodes 5 and 6 whilst r with nodes 1, 2, 3 and 4.

The solution of the second submatrix equation of Eq.(23) for $\hat{\mathbf{d}}_c$ yields

$$\hat{\mathbf{d}}_c = \hat{\mathbf{K}}_{cc}^{-1}\left(\hat{\mathbf{P}}_c - \hat{\mathbf{K}}_{cr}\hat{\mathbf{d}}_r\right) \tag{24}$$

Substituting Eq.(24) into the first submatrix equation of Eq.(23) to eliminate $\hat{\mathbf{d}}_c$ leads to

$$\hat{\mathbf{K}}'_e\hat{\mathbf{d}}'_e = \hat{\mathbf{P}}'_e \tag{25}$$

where

$$\hat{\mathbf{K}}'_e = \hat{\mathbf{K}}_{rr} - \hat{\mathbf{K}}_{rc}\hat{\mathbf{K}}_{cc}^{-1}\hat{\mathbf{K}}_{rc}^T, \quad \hat{\mathbf{P}}'_e = \hat{\mathbf{P}}_r - \hat{\mathbf{K}}_{rc}\hat{\mathbf{K}}_{cc}^{-1}\hat{\mathbf{P}}_c \tag{26a,b}$$

The elimination process from Eq.(23) to Eq.(25) is completed by static condensation [24]. Here, $\hat{\mathbf{K}}'_e$ and $\hat{\mathbf{P}}'_e$ are, respectively, the equivalent stiffness matrix and nodal force vector of KL interface element.

For solution purpose, the KL element stiffness equation (25) must be transformed into the form in the global Cartesian coordinate system (X,Y) so that

$$\hat{\mathbf{K}}_e\hat{\mathbf{d}}_e = \hat{\mathbf{P}}_e \tag{27}$$

together with

$$\hat{\mathbf{K}}_e = \left[\mathbf{R}^*\right]^T\hat{\mathbf{K}}'_e\mathbf{R}^*, \quad \hat{\mathbf{P}}_e = \left[\mathbf{R}^*\right]^T\hat{\mathbf{P}}'_e \tag{28a,b}$$

$$\hat{\mathbf{d}}_e = \{u_{1X} \quad u_{1Y} \quad u_{2X} \quad u_{2Y} \quad u_{3X} \quad u_{3Y} \quad u_{4X} \quad u_{4Y}\}^T \tag{28c}$$

in which

$$\mathbf{R}^* = \text{diag}[\mathbf{R} \quad \mathbf{R} \quad \mathbf{R} \quad \mathbf{R}] \text{ with } \mathbf{R} = \begin{Bmatrix} \cos\theta & \sin\theta \\ -\sin\theta & \cos\theta \end{Bmatrix} \tag{29}$$

2.3 Interface model and numerical implementation

Fig.4 shows a contact interface model, where a prospective contact zone Ω^C may be bounded by the boundaries Γ_c^A, Γ_c^B, Γ_1 and Γ_2. 4-node KL interface elements are embedded in the prospective contact zone for simulating the behaviour of interaction.

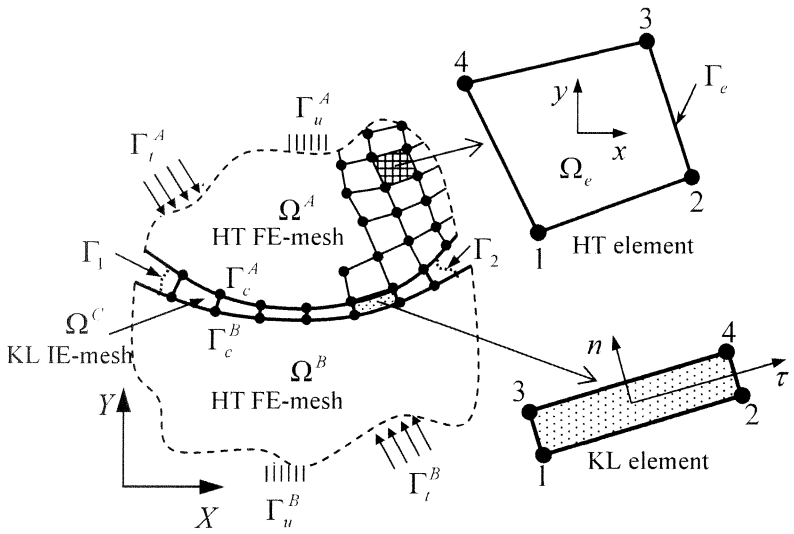

Fig. 4 Two HT element subdomains in contact with KL elements

In order to evaluate contact non-linearity, an appropriately interfacial constitutive relation, namely normal and tangential stress-relative displacement curves, is established for the KL element (see Fig.5). In accordance with Fig.4, the corresponding stresses σ_τ , σ_n in Eq.(18) can be rewritten as follows

$$\sigma_n = \begin{cases} 0 & \text{if } w_n > 0 \quad \text{sepration} \\ k_n w_n & \text{otherwise} \quad \text{contact} \end{cases} \tag{30a}$$

$$\sigma_\tau = \begin{cases} 0 & \text{if } w_n > 0 \quad \text{sepration} \\ k_\tau w_\tau & \text{if } w_n \le 0 \text{ and } |w_\tau| \le -\mu \frac{k_n}{k_\tau} w_n \quad \text{stick} \\ -\mu k_n w_n & \text{if } w_n \le 0 \text{ and } |w_\tau| > -\mu \frac{k_n}{k_\tau} w_n \quad \text{slip} \end{cases} \tag{30b}$$

It is clear from Eq.(30b) that the classical Coulomb friction law is considered for tangential behaviour of the interface. In addition, special attention must be paid to the choice of the optimum values of penalty parameters k_τ, k_n. Excessively high values tend to provide ill-conditioned numerical problem whilst too small values could not prevent the penetration between the two contacting bodies. Although automatic calculations of the penalty parameters have been reported in the literature [25,26], these approaches have some limitations, such as not taking into account of the separation mode or frictional effects across the interface in the analysis. Therefore, in the next section a parametric study on k_τ, k_n will be carried out in detail through numerical examples.

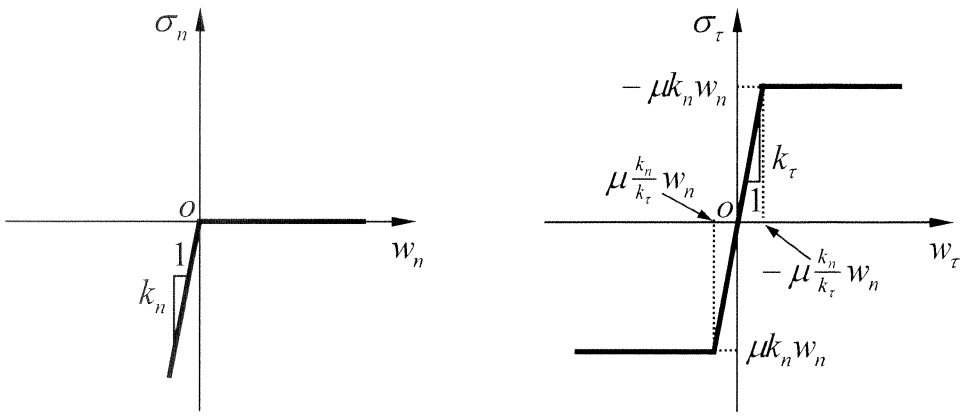

(a) Normal direction (b) Tangential direction

Fig. 5 Schematic representation of interfacial constitutive relation

The HT FE-interface model for contact problems has been implemented in ABAQUS via user element subroutine (UEL) including both HT and KL elements. The iterations for calculating the stresses of Eqs.(30a,b) at the interface are completed within the UEL.

3 Numerical examples

In order to assess the HT FE-interface contact model developed in this paper, two benchmark examples were considered. The assumption of plane strain condition was made in the subsequent analyses. It should be noted that all results obtained from ABAQUS are based on the contact property options: "hard" contact pressure-overclosure and penalty friction formulation.

Example 1. A block resting on a substratum

As shown in Fig.6, a block is pressed on a substratum with the pressure of $q = 100\,\text{MPa}$ on its top surface. The geometry and boundary conditions are also shown in the figure. Material properties of both bodies are the same with Young's modulii $E^A = E^B = 2000\,\text{MPa}$ and Poisson's ratios $v^A = v^B = 0.3$.

Three different meshes used in the analyses are illustrated in Fig.7. Care was taken to keep the mesh density fine in the vicinity of singularity point P and the potential stick-slip boundary in all cases of meshing. Table 1 shows the mesh properties, the CPU time and convergence of displacements and shear stress at point P. Although the problem is very small, the saving in CPU time is apparent with the use of the HT FE and KL interface element modelling against the current ABAQUS surface contact modelling technique. In complex problems, the reduction in CPU time might be significant.

Mesh	No. of Elements		CPU time (s)		Horizontal Disp. (mm)		Vertical Disp. (mm)		Shear Stress (MPa)	
	HT	KL	Abaqus	Present	Abaqus	Present	Abaqus	Present	Abaqus	Present
1	396	28	21	20	0.835	0.836	-0.685	-0.682	36.466	35.452
2	1044	36	25	23	0.816	0.814	-0.689	-0.687	31.075	30.764
3	3096	52	35	33	0.806	0.810	-0.692	-0.695	28.715	28.077

Table 1: Mesh properties, CPU time and convergence for Example 1

Since the interface penalty stiffnesses k_τ and k_n play a significant role in the numerical analysis, their influence on the contact behaviour was first examined. First, normal stiffness to elastic modulus ratio was varied from 0.5 (soft interface) to 50 (hard interface) for frictionless contact and the results are shown in Fig. 8.

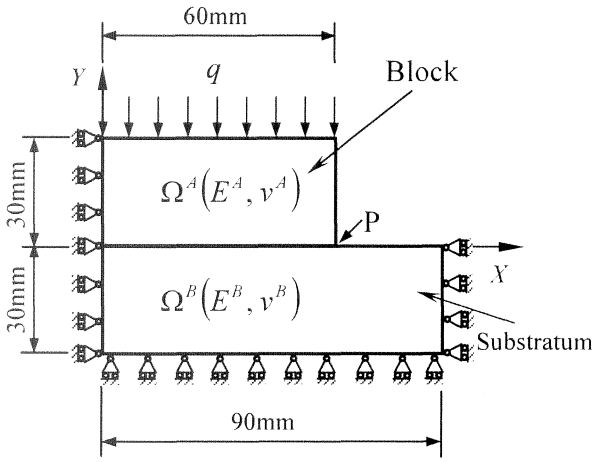

Fig. 6 A block resting on a substratum

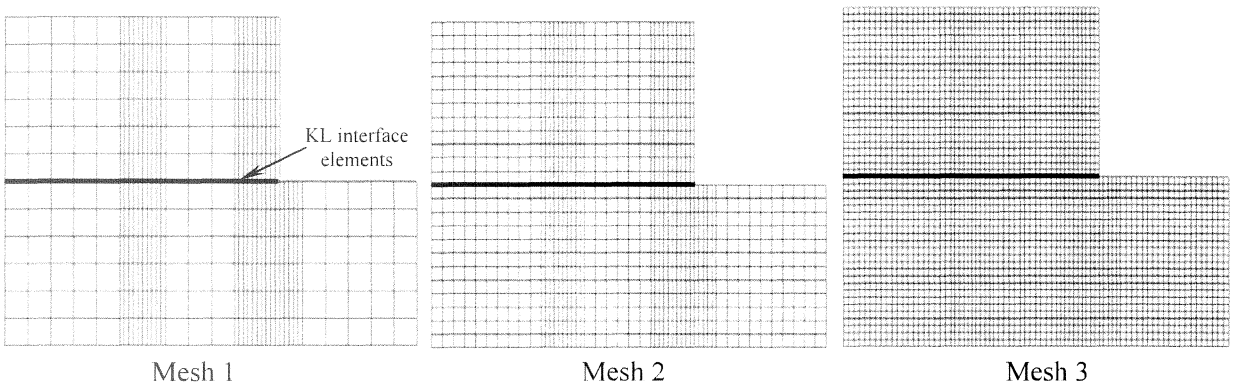

Fig. 7 Mesh convergence studies

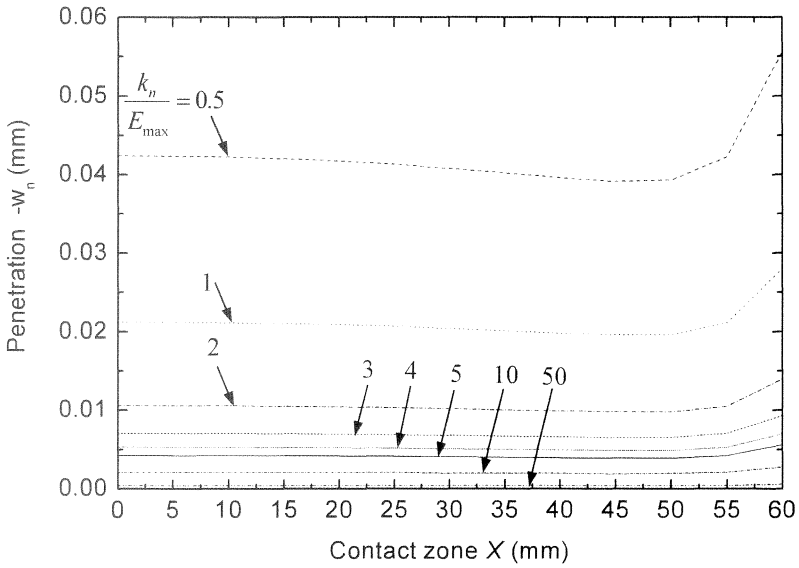

Fig. 8 Effect of k_n on the penetration in the frictionless case

Fig.8 shows the penetrations of the KL elements along the interface for a wide range of the ratio of normal stiffness to Young's modulus $\left(\frac{k_n}{E_{\max}}\right)$ in the frictionless case, where $E_{\max} = \max\left(E^A, E^B\right)$. It can be observed that as the ratio $\frac{k_n}{E_{\max}}$ increases from $0.5 \sim 50$ the penetration decreases. To search an appropriate value of k_n, an error norm was defined as follows:

$$\text{Error} = \max\left(\frac{w_n}{u_n^{top}}, \frac{w_n}{u_n^{bot}}\right)_{sp} \times 100\% \tag{31}$$

where the subscript sp stands for the sampling (or herein Simpson) points.

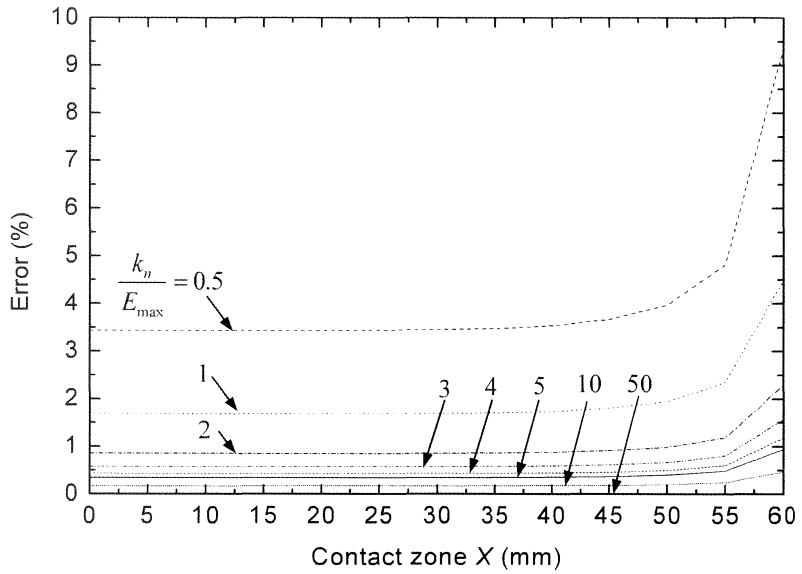

Fig. 9 Error of penetration for different k_n in the frictionless case

From Fig.9, it can be seen that for $\frac{k_n}{E_{\max}} \geq 3$ the maximum error has remained less than 2% which is acceptable for most practical applications. Therefore, a reasonable choice for k_n may be postulated as

$$k_n = (3 \sim 5)E_{\max} \tag{32}$$

Note that Eq.(32) is just an equality in magnitude or an empirical relationship, the coefficient has length dimension (mm). In this paper we have chosen the relation $k_n = 5E_{\max}$ for all the analyses.

Next a frictional case with a frictional coefficient $\mu = 0.1$, as illustrated in Fig.10, was considered. The penalty normal stiffness was chosen as $k_n = 10^4$ N/mm whilst three penalty tangential stiffnesses of k_τ were employed: $10^2, 10^3$ and 10^4 N/mm, namely $\frac{k_n}{k_\tau} = 100, 10$ and 1 in the HT FE-interface analysis for investigation of optimal value. Comparison of the results indicates that the choice of $\frac{k_n}{k_\tau} = 10$ can capture the contact behaviour accurately. In order to verify the convergence of the HT FE-interface model, numerical calculations have been carried out with different meshes (see Fig.6) for $\frac{k_n}{k_\tau} = 10$. The results in Fig.11 illustrate good agreement with the results of the conventional FE modelling obtained from ABAQUS with increase of the density of mesh.

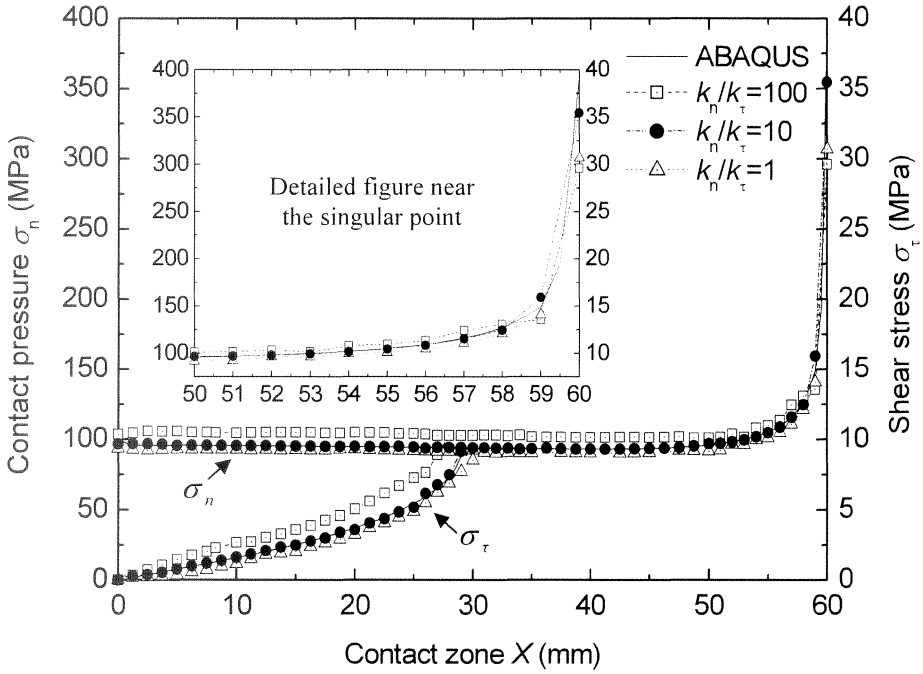

Fig. 10 Effect of interface stiffnesses on the contact behaviour ($\mu = 0.1$)

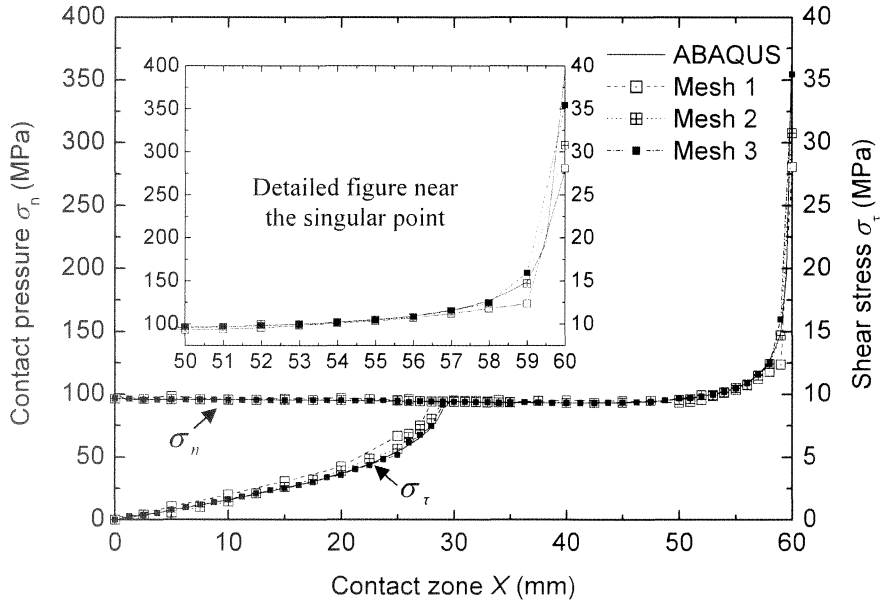

Fig.11 Convergence study of different meshes ($k_n / k_\tau = 10; \mu = 0.1$)

In Fig. 10 and Fig. 11, the variation of normal and shear stress in the contact zone (determined by the KL interface element) is graphically illustrated. The effect of meshing and the ratio of normal to tangential stiffness are presented in Figs 11 and 10 respectively. It could be seen that the normal stress (pressure) in the contact zone almost remained constant except the last 5mm length of contact (singularity zone). The shear stress, on the other hand exhibits rapid raise from zero to a compatible value to normal stress. The point where the shear stress curve meets the normal stress curve is thurs regarded as the point of separation of the slip zone from the stick zone.

Example 2. An inclusion inserted in an infinite plate

An inclusion problem subjected to a uniform tension of q=1000MPa together with geometry and boundary conditions is shown in Fig.12. The radius r of inclusion with perfect fit to the hole of an infinite plate was set as 25.4mm. Linear elastic material properties characterized by Young's modulus of 4000MPa and Poisson's ratio of 0.35 were taken for both constituent bodies.

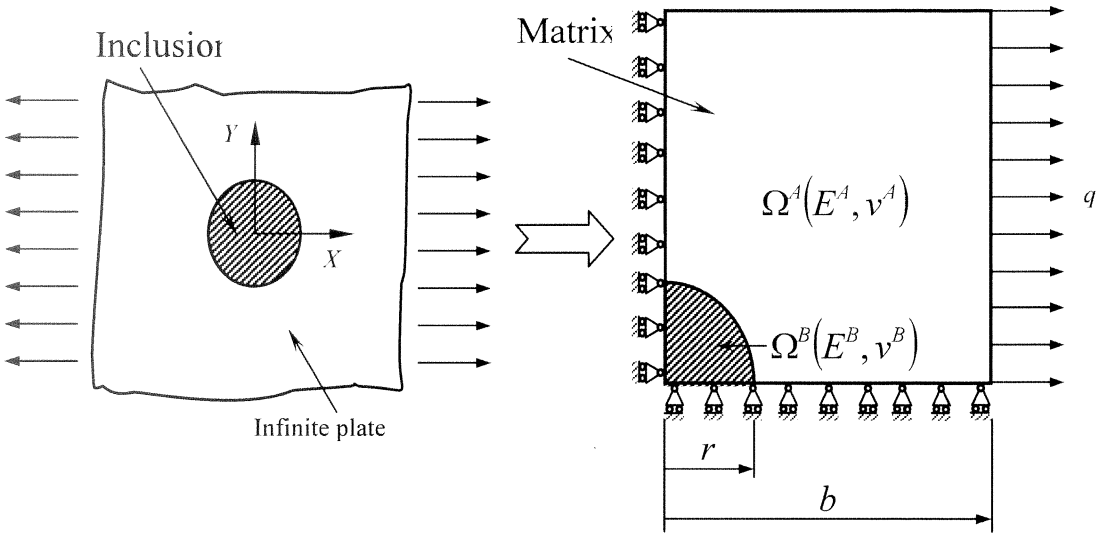

(a) Infinite model (b) Finite model

Fig. 12 An inclusion inserted in an infinite plate and its simplified model

For numerical purpose a simplified finite element model was employed (see Fig.12(b)). Due to symmetry, only a quarter of the problem has been discretised. The simplified model consisted of 8231 HT elements and 40 KL interface elements (each of 0.52mm long). To conform to the results given in the literature [27,28], the frictionless case was first considered. Based on the parametric study of Example 1, $k_n = 2\times10^4$ N/mm was used in the following analysis and the corresponding mesh is used for Example 2 shown in Fig.13. As only the contact zone was of interest, the contact zone was meshed using high density elements with the other regions meshed with course element size.

Fig.14 presents the results with a range of size of inclusion size to matrix size, expressed as ratios of r/b=0.5, 0.2, 0.1, 0.083 and 0.05. Numerical results presented in Fig.14 reveal that the real contact arc and the maximum contact pressure decrease with the reduction in r/b. A stable value of 19.62° and 609MPa predicted by Stippes et al [27] was apparently achieved in this analysis as shown in Fig.14. For the ratio r/b=0.083, the results (stable contact angle and the corresponding contact pressure) did not change substantially. It can therefore be claimed that in this study, we have reconfirmed the ratio of r/b=0.083 represented an infinite model shown in Fig.12(a) accurately, as proved earlier by Knight et al[28].

The results for a frictional coefficient of $\mu = 1.8$ (representing rough contact or snug fit) are presented in Fig.15. In the HT FE-interface analysis the penalty normal and tangential stiffnesses were respectively chosen as $k_n = 2\times10^4$ N/mm and $k_\tau = 2\times10^3$ N/mm . Comparison of the results was made between the present model and conventional FE model (ABAQUS) and only small deviations have been found. It is also found that the maximum contact pressure decreases due to the influence of friction but the real contact arc remains almost identical to that in the frictionless case.

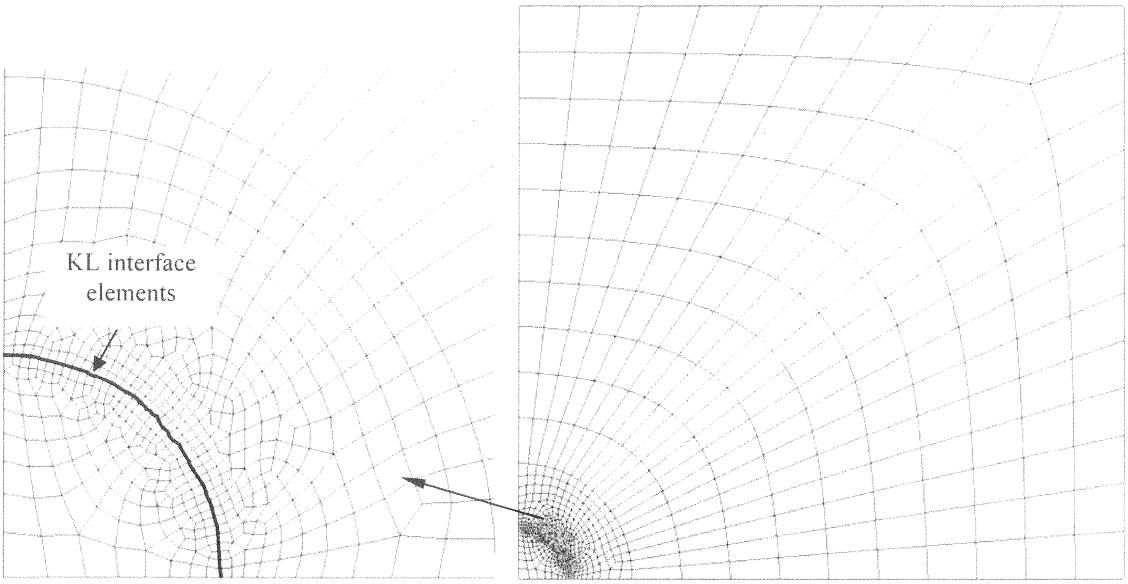

Fig.13 Configuration of mesh for Example 2 (r/b=0.083)

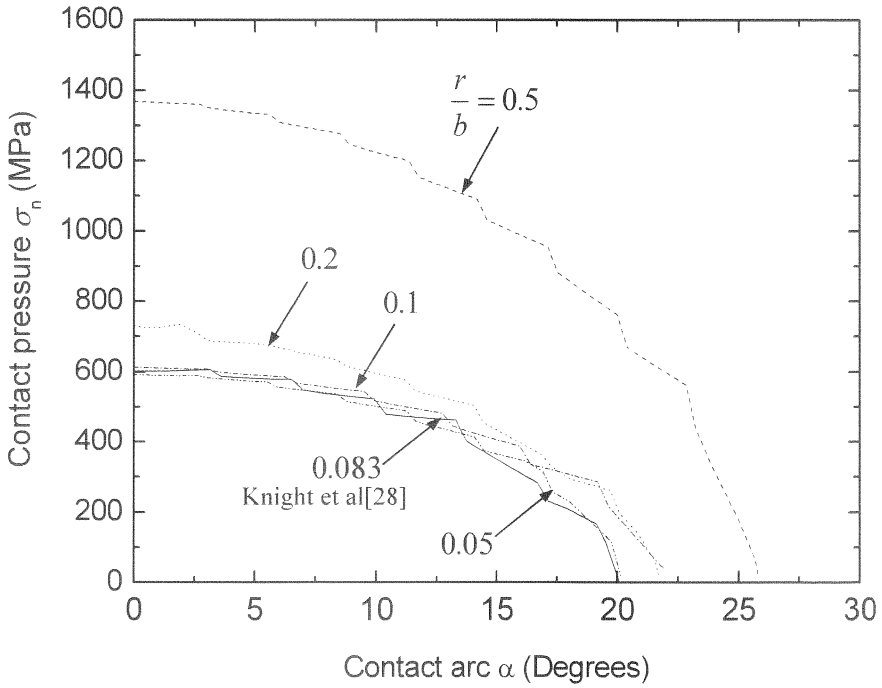

Fig. 14 Effect of r/b on the contact behaviour in the frictionless case

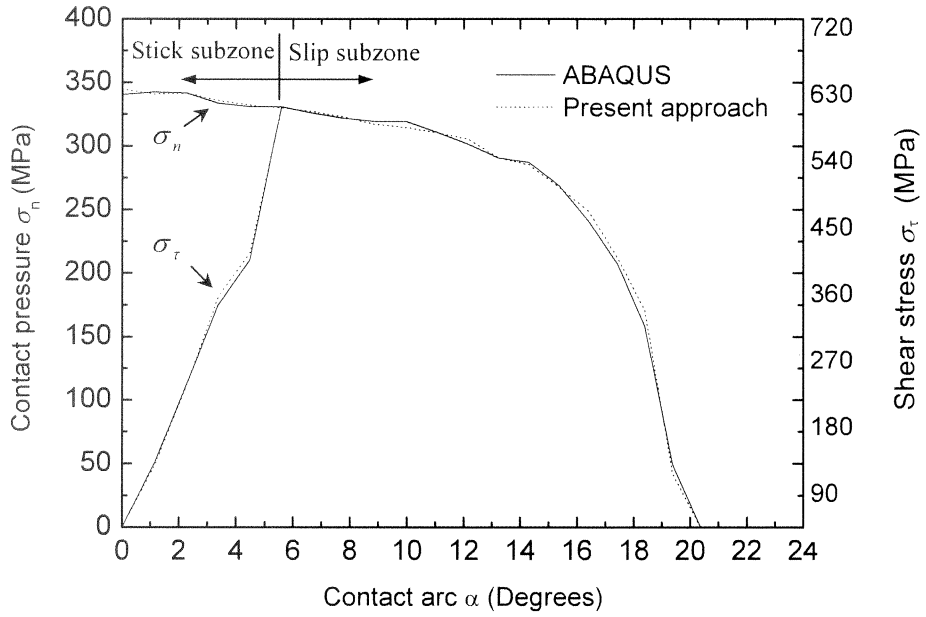

Fig. 15 Contact behaviour of Knight model in the frictional case (r/b=0.083, $\mu = 1.8$)

4 Concluding remarks

An interface model for elastic contact problems using HT FE has been developed in this paper. Four-noded HT elements were formulated and used in the discretisation of the contacting bodies whereas four-noded KL interface elements were formulated and embedded in the prospective contact zone for simulating the behaviour of interaction. In order to ensure better performance of the KL element in the analysis of contact problems, an interfacial constitutive relation, viz. normal and tangential stress vs relative displacement curves, was appropriately facilitated. Additionally, the Simpson-type Newton-Cotes integration scheme has been utilized for the KL element stiffness equation.

The HT FE-interface model was implemented in the ABAQUS (via UEL). Two benchmark examples were investigated and all computed results have proved their reliability with respect to the relevant analytical or conventional FE (ABAQUS) solutions. Especially, the effect of penalty stiffnesses on the results and the characteristic of convergence have been studied in detail.

Further extension of the model to 3D case is feasible once the 3D HT FE and interface elements are introduced.

Appendix A. Trefftz function matrix $\mathbf{N}_e$

According to Muskhelishvili's complex variable formulation, a complete system of homogeneous solutions, namely Trefftz functions $\mathbf{N}_{ej}$ can be generated in a systematic way. For conciseness, only the results are listed below

$$\mathrm{N}_{ej} = \frac{1}{2\mathrm{G}} \begin{Bmatrix} \mathrm{Re}\, Z_{1k} \\ \mathrm{Im}\, Z_{1k} \end{Bmatrix}, \quad Z_{1k} = i\kappa z^k + kiz\bar{z}^{k-1} \tag{A.1}$$

$$\mathrm{N}_{ej+1} = \frac{1}{2\mathrm{G}} \begin{Bmatrix} \mathrm{Re}\, Z_{2k} \\ \mathrm{Im}\, Z_{2k} \end{Bmatrix}, \quad Z_{2k} = \kappa z^k - kz\bar{z}^{k-1} \tag{A.2}$$

$$N_{ej+2} = \frac{1}{2G}\begin{Bmatrix} \mathrm{Re}\, Z_{3k} \\ \mathrm{Im}\, Z_{3k} \end{Bmatrix}, \quad Z_{3k} = i\bar{z}^{k} \tag{A.3}$$

$$N_{ej+3} = \frac{1}{2G}\begin{Bmatrix} \mathrm{Re}\, Z_{4k} \\ \mathrm{Im}\, Z_{4k} \end{Bmatrix}, \quad Z_{4k} = -\bar{z}^{k} \tag{A.4}$$

where $z = x_1 + ix_2$, $\bar{z} = x_1 - ix_2$, $i = \sqrt{-1}$, $k = 1,2,\cdots$.

Appendix B. Derivation of the element stiffness equation

The element stiffness equation can be formulated by setting $\delta\Pi_{me} = 0$ or $\delta\Psi_{me} = 0$. Using divergence theorem, the functional Π_{me} can be rewritten as in (B.1)

$$\Pi_{me} = \tfrac{1}{2}\iint_{\Omega_e} \bar{b}_i u_i \,\mathrm{d}\Omega + \tfrac{1}{2}\int_{\Gamma_e} t_i u_i \,\mathrm{d}\Gamma - \int_{\Gamma_{eu}} t_i \bar{u}_i \,\mathrm{d}\Gamma - \int_{\Gamma_{eu}} (t_i - \bar{t}_i)\tilde{u}_i \,\mathrm{d}\Gamma - \int_{\Gamma_{el}} t_i \tilde{u}_i \,\mathrm{d}\Gamma \tag{B.1}$$

By substituting Eqs.(2a,b) and (11) into (B.1), we obtain

$$\Pi_{me} = \tfrac{1}{2}\mathbf{c}_e^T \mathbf{H}_e \mathbf{c}_e + \mathbf{c}_e^T \mathbf{G}_e \mathbf{d}_e + \mathbf{c}_e^T \mathbf{h}_e + \mathbf{d}_e^T \mathbf{g}_e + \text{terms without } \mathbf{c}_e \text{ and } \mathbf{d}_e \tag{B.2}$$

where

$$\mathbf{H}_e = \int_{\Gamma_e} \mathbf{Q}_e^{\mathrm{T}} \mathbf{N}_e \,\mathrm{d}\Gamma = \int_{\Gamma_e} \mathbf{N}_e^{\mathrm{T}} \mathbf{Q}_e \,\mathrm{d}\Gamma \tag{B.3}$$

$$\mathbf{G}_e = \int_{\Gamma_{el} \cup \Gamma_{el}} \mathbf{Q}_e^{\mathrm{T}} \tilde{\mathbf{N}}_e \,\mathrm{d}\Gamma \tag{B.4}$$

$$\mathbf{h}_e = -\frac{1}{2}\iint_{\Omega_e} \mathbf{N}_e^{\mathrm{T}} \bar{\mathbf{b}}_e \,\mathrm{d}\Omega - \frac{1}{2}\int_{\Gamma_e} \left(\mathbf{Q}_e^{\mathrm{T}} \bar{\mathbf{u}}_e + \mathbf{N}_e^{\mathrm{T}} \breve{\mathbf{t}}_e\right)\mathrm{d}\Gamma + \int_{\Gamma_{eu}} \mathbf{Q}_e^{\mathrm{T}} \bar{\mathbf{u}} \,\mathrm{d}\Gamma \tag{B.5}$$

$$\mathbf{g}_e = \int_{\Gamma_{el}} \tilde{\mathbf{N}}_e^{\mathrm{T}} (\bar{\mathbf{t}}_e - \breve{\mathbf{t}}_e) \,\mathrm{d}\Gamma - \int_{\Gamma_{el}} \tilde{\mathbf{N}}_e^{\mathrm{T}} \bar{\mathbf{t}}_e \,\mathrm{d}\Gamma \tag{B.6}$$

Note that numerical integrals in (B.3-B.6) are performed using Gaussian quadrature rule. In absence of body forces $\mathbf{h}_e$ vanishes while $\mathbf{g}_e$ is evaluated by the following simple form

$$\mathbf{g}_e = -\int_{\Gamma_{el}} \tilde{\mathbf{N}}_e^{\mathrm{T}} \bar{\mathbf{t}}_e \,\mathrm{d}\Gamma \tag{B.7}$$

To enforce inter-element continuity on the common element boundary, the unknown vector $\mathbf{c}_e$ should be expressed in terms of nodal DOF $\mathbf{d}_e$. An optional relationship between $\mathbf{c}_e$ and $\mathbf{d}_e$ in the sense of variation can be evaluated as

$$\frac{\partial \Pi_{me}}{\partial \mathbf{c}_e} = 0 \quad \Rightarrow \quad \mathbf{c}_e = \mathbf{H}_e^{-1}\left(\mathbf{G}_e \mathbf{d}_e + \mathbf{g}_e\right) \tag{B.8}$$

Substituting (B.7) into (B.2) and making similar manipulation yields the element stiffness equation

$$\frac{\partial \Pi_{me}}{\partial \mathbf{d}_e} = 0 \quad \Rightarrow \quad \mathbf{K}_e \mathbf{d}_e = \mathbf{P}_e \tag{B.9}$$

Appendix C. Newton-Cotes integration scheme

The general form of Newton-Cotes rules can be written as follows:

$$\int_a^b f(x)dx \cong C_o h \sum_{i=1}^{n} W_i f(x_i) + C_1 h^{k+1} f^{(k)}(\zeta) \tag{C.1}$$

where ζ represents a value of x in the range of integration, and h represents the distance between adjacent sampling points. A summary of the values of C_o, C_1, the W_i's and k for the first five formulae in the Newton-Cotes series is given in Table C.1.

n	C_o	W_1	W_2	W_3	W_4	W_5	C_1	k	Name
1	1	1					$\frac{1}{2}$	1	Rectangle
2	$\frac{1}{2}$	1	1				$-\frac{1}{12}$	2	Trapezium
3	$\frac{1}{3}$	1	4	1			$-\frac{1}{90}$	4	Simpson
4	$\frac{3}{8}$	1	3	3	1		$-\frac{3}{80}$	4	4-point
5	$\frac{2}{45}$	7	32	12	32	7	$-\frac{8}{945}$	6	5-point

Table C.1: Summary of Newton-Cotes rules

References

[1] R.E. Goodman, R.L. Tylor, T.L. Brekke. A model for mechanics of jointed rock. *J. Soil Mech. Foundation ASCE* , **94**: 19-43, 1968.

[2] R.A. Day, D.M. Potts. Zero thickness element-numerical stability and application. *Int. J. Number Meth. Anal. Geomech.*, **18**: 689-708, 1994.

[3] A. Gens, I. Carol, E.E. Alonso. An interface element formulation for the analysis of soil reinforcement interaction. *Computers and Geotechnics,* **7**: 133-151, 1988.

[4] X.Y. Lei. Contact friction analysis with a simple interface element. *Comput. Methods Appl. Mech. Engrg.*, **190**: 1955-1965, 2001.

[5] J.C.J. Schellekens, R.D. Borst. On the numerical integration of interface elements. *Int. J. Solids Struct.*, **36**: 43-66,1993.

[6] L.R. Herrmann. Finite element analysis of contact problems. *J. Eng. Mech. ASCE,* **104**: 1043-1059, 1978.

[7] V.N. Kaliakin, J. Li. Insight into deficiencies associated with commonly used zero-thickness interface elements. *Computers and Geotechnics*, **17**: 225-252, 1995.

[8] Q.H. Qin. *The Trefftz Finite and Boundary Element Method.* WIT Press, Southampton, 2000.

[9] J. Jirousek, N. Leon. A powerful finite element for plate bending. *Comput. Methods Appl. Mech. Eng.*, **12**: 77-96, 1977.

[10] J. Jirousek, P. Teodorescu. Large finite element method for the solution of problems in the theory of elasticity. *Comput. Struct.*, **15**: 575-587, 1982.

[11] J. Jirousek, A. Venkatesh. Hybrid Trefftz plane elasticity elements with *p*-method capabilities. *Int. J. Numer. Meth. Engng.*, **35**: 1443-1472, 1992.

[12] J.A.T. Freitas, Z.M. Wang. Hybrid-Trefftz stress elements for ealstoplasticity. *Int. J. Numer. Meth. Engng.*, **43**: 655-683, 1998.

[13] Q.H. Qin. Formulation of hybrid Trefftz finite element method for elastoplasticity. *Applied Mathematical Modelling*, **29**: 235-252, 2005.

[14] J. Jirousek, L. Guex. The hybrid-Trefftz finite element model and its application to plate bending. *Int. J. Num. Meth. Engng.*, **23**: 651-693, 1986.

[15] Q.H. Qin. Hybrid-Trefftz finite element method for Reissner plates on an elastic foundation. *Comp. Meth. Appl. Mech. Eng.*, **122**: 379-392, 1995.

[16] J. Jirousek, Q.H. Qin. Application of hybrid-Trefftz element approach to transient heat conduction analysis. *Comput. Struct.*, **58**: 195-201, 1996.

[17] Q.H. Qin. Variational formulations for TFEM of piezoelectricity. *Int. J. Solids Struct.*, **40**: 6335-6346, 2003.

[18] Q.H. Qin. Solving anti-plane problems of piezoelectric materials by the Trefftz finite element approach. *Computational Mechanics*, **31**: 461-468, 2003.

[19] Ch. Hochard. A Trefftz approach to computational mechanics. *Int. J. Numer. Meth. Engng.*, **56**: 2367-2386, 2003.

[20] K.Y. Wang, Q.H. Qin, K.L. Kang, J.S. Wang. A direct constraint-Trefftz FEM for analyzing elastic contact problems. *Int. J. Numer. Meth. Engng.*, 2005. in press

[21] D.V. Griffiths, I.M. Smith. *Numerical methods for engineers*. Black scientific publications, London, 1991.

[22] K.Y. Wang, Q.H. Qin, K.L. Kang. A modified isoparametric mapping fill method to display color mapping of data. *Advances in Engineering Software*, **35**: 585-591, 2004.

[23] Q.H. Qin. Dual variational formulation for Trefftz finite element method of elastic materials. *Mechanics Research Communications*, **31**: 321-330, 2004.

[24] E. Wilson. The static condensation algorithm. *Int. J. Numer. Meth. Engng.*, **8**: 199-203, 1974.

[25] A. Pantano, R.C. Averill. A penalty-based finite element interface technology. *Comput Struct.*, **80**: 1725-1748, 2002.

[26] D. Chamoret, P. Saillard, A. Rassineux, J.M. Bergheau. New smoothing procedures in contact mechanics. *Journal of Computational and Applied Mathematics*, **168**: 107-116, 2004.

[27] M. Stippes, H.B. Wilson, F.N. Jr Krull. A contact stress problem for a smooth disk in an infinite plate. In: Proceedings of the 4th U.S. National Congress of Applied Mechanics, ASME, 799-806, 1962.

[28] M.G. Knight, L.A. Lacerda, L.C. Wrobel, J.L. Henshall. Parametric study of the contact stresses around spherical and cylindrical inclusions. *Computational Materials Science*, **25**: 115-121, 2002.